Nanotechnology

DOI: 10.1002/anie.200902114

Long-Range, High-Resolution Magnetic Imaging of Nanoparticles**

*Li Yao and Shoujun Xu**

Magnetic nanoparticles are widely used as biochemical markers, drug-delivery carriers, and imaging contrast agents.[1] The precise determination of the position and number of particles in a sample at a given time is vital for these purposes. In many applications, such as assay analysis on microchips and in vivo imaging,[2,3] the magnetic particles are far from the detectors, on the order of several millimeters to a few centimeters. This makes it challenging to obtain desired spatial information and sufficient detection limit because of the dependence of magnetic field strength on r^{-3}, where r is the distance between the sample and the detector.

Successful imaging of magnetic nanoparticles in practical settings must fulfill two criteria. One is high sensitivity in detecting a dc magnetic field. The other is the capability of resolving spatial information at a long detection distance. Various magnetic force microscopy and magnetic resonance force microscopy techniques,[4] which usually have a detection range of around a few nanometers or less, are thus not suitable for these applications. Similarly, room-temperature giant magneto-resistive sensors are applicable only when the sensor is placed within a few micrometers of the sample.[5] Large-scale magnetic imaging modalities often lack sensitivity because of the distance dependence of the magnetic field and magnetic response; the reduced sensitivity requires the use of impractical amounts of sample.[6] Indirect detection of magnetic particles has also been investigated. Optical detection offers high sensitivity, but it requires a transparent environment, which is not possible in many cases.[7] Separately, conventional magnetic resonance imaging offers high spatial resolution through encoding with gradient magnetic fields, but the drawbacks include poor sensitivity to dc magnetic fields and the requirement of a superconducting magnet.[8]

Atomic magnetometry is one of the most sensitive techniques for measuring dc magnetic fields.[9] Unlike the rival superconducting magnetometers or cryogenically cooled giant magneto-resistive sensors,[10,11] the use of atomic magnetometers is facilitated by the fact that they require no cryogenics. Atomic magnetometers have been used to detect magnetic particles; however, no spatial information was extracted, nor could the amount of the sample be determined.[12] Since the magnetic field is a function of both the number of nanoparticles and their distance from the detector, it is difficult to resolve spatial information without prior knowledge of the amount of the sample.

To address this problem, we present a scanning imaging method that utilizes a novel atomic magnetometer to generate a map of the magnetic field. From the full magnetic field profile, instead of a single-point measurement, we demonstrate that the spatial information can be resolved, and the amount of the magnetic sample can be obtained simultaneously. Furthermore, we perform a series of scans to obtain a two-dimensional magnetic image of the sample, which demonstrates the accuracy of the distance measurement and the reproducibility of the measured amount of the magnetic sample.

Scheme 1 shows the experimental configuration. A cesium-based atomic magnetometer is located several millimeters away from an assemble of magnetic nanoparticles to be measured. The magnetic sample can be scanned both perpendicular to the propagation of the laser (x axis) and parallel to the laser (d axis). The atomic magnetometer measures the magnetic field generated by the nanoparticles at each position during the scans. The result for a single scan along the x direction is shown in Figure 1.

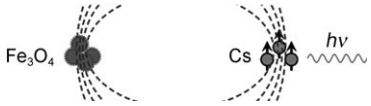

Scheme 1. Imaging of magnetic nanoparticles at a long distance. A laser beam generates ground-state coherence in Cs atoms, which rotates the polarization of the incident laser beam. The degree of rotation is a measure for the magnetic field of the sample.

Without prior knowledge of the precise amount of the sample or its distance from the Cs detector, we show that analyzing this profile yields both spatial information and the amount of the magnetic sample. Based on the experimental geometry and since the magnetic field corresponds to the overall dipolar field of the sample particles, the profile follows Equation (1). Here, B is the magnetic field measured by the magnetometer, and B_0 is the baseline correction. The symbol x_0 represents the position on the x axis that corresponds to the maximum signal, which is normalized to zero in Figure 1 for convenience. M is the magnetization of the magnetic particles, and d is the distance between the sample and the detector. By performing a least-square fit on the magnetic field profile, we obtain both the magnetization of the particles and the

$$B = B_0 + \frac{\mu_0 M}{4\pi((x-x_0)^2+d^2)^{3/2}}\left(3\frac{d^2}{(x-x_0)^2+d^2}-1\right) \quad (1)$$

[*] Dr. L. Yao, Prof. S. Xu
Department of Chemistry, University of Houston
Houston, TX 77204 (USA)
Fax: (+1) 713-743-2709
E-mail: sxu7@uh.edu
Homepage: http://www.chem.uh.edu/Faculty/Xu/

[**] This work is supported by a startup fund and a GEAR grant from the University of Houston. L.Y. acknowledges support by the McElrath Fellowship.

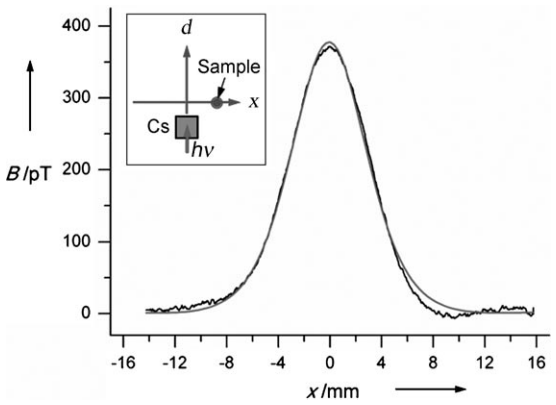

Figure 1. Magnetic field profile of an assembly of approximately 7×10^5 magnetic nanoparticles (experimental data and fitted curve). The inset shows the geometry of the scanning axes with respect to the laser beam and the Cs detector.

distance between the sample and the detector: $(5.589\pm0.047)\times10^{-10}\,\mathrm{A\,m^2}$ and (6.709 ± 0.020) mm, respectively. We would like to point out that since atomic magnetometers directly measure the absolute value of magnetic fields, the magnetization value needs no calibration.

To demonstrate two-dimensional scanning imaging, we performed a series of x-axis scans at different distances. The d values were varied in increments of 100 μm by moving the nanopositioning stages that hold the sample. The magnetic field is a function of both the x position, which is controlled by a linear actuator, and the d position, which is obtained from the experimental magnetic profile. The resulting two-dimensional image is shown in Figure 2. The maximum value of the magnetic field (at $x=0$) decreases as the sample moves farther from the detector. Because of the small amount of the sample and the large separation between the sample and the detector, the amplitude of the signal is several hundreds of picotesla—much smaller than the signal in magnetic force microscopy.

From the two-dimensional image, we first examine the accuracy of the d parameters obtained from fitting the magnetic field profile. The fitted d values are listed in Table 1, along with the readings from the nanopositioning stages for comparison. The error bars are all less than 23 μm. Importantly, from the relative distance movement Δd, the values obtained from the image agree well with the readings from the nanopositioning stages. The accuracy is within 15 μm.

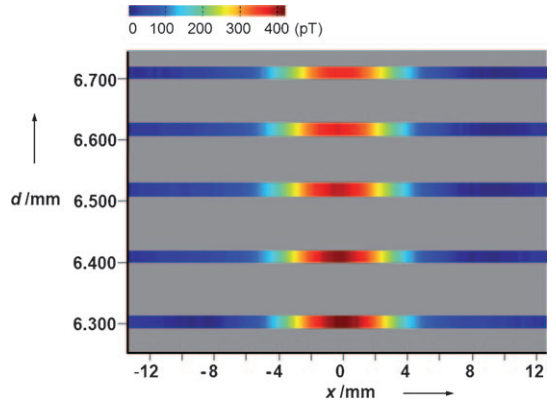

Figure 2. A two-dimensional scanning magnetic image. Each stripe represents an x-axis scan. The width of each stripe is determined by the corresponding error bar of the fitted d value.

Table 1: Comparison between the stage movement and fitted distance values, d, and measured magnetization results, M.

Stage [mm][a]	d [mm]	Δd [mm]	M [10^{-10} A m^2]
0	6.304 ± 0.020	0	5.353 ± 0.049
0.100	6.408 ± 0.020	0.104	5.415 ± 0.048
0.200	6.519 ± 0.023	0.215	5.505 ± 0.054
0.300	6.616 ± 0.022	0.311	5.551 ± 0.051
0.400	6.709 ± 0.020	0.405	5.589 ± 0.047

[a] The stage positions are relative values to the position of the first measurement, which is set as 0.

In addition to the spatial information, we compare the magnetization values obtained from different x scans. Since the imaging scans are performed with a fixed number of magnetic particles, the magnetization obtained at different distances should be the same (within experimental error). Figure 3 plots the resulting M values as a function of relative distance Δd, which represents different x scans. For each fit, the error bar is within 1%. The average magnetization for the five x scans is $5.483\times10^{-10}\,\mathrm{A\,m^2}$, with a standard deviation of $0.097\times10^{-10}\,\mathrm{A\,m^2}$, which is less than 1.8% of the average.

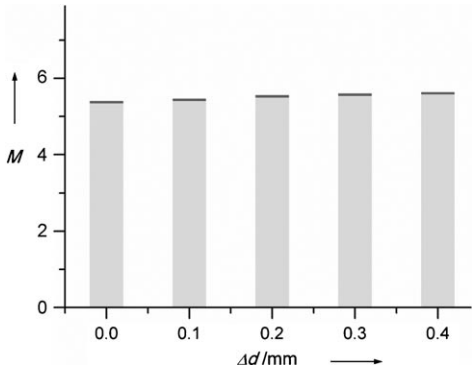

Figure 3. Fitted magnetizations of the sample for the different x scans which are indicated using relative distances, Δd. M: magnetization, in $10^{-10}\,\mathrm{A\,m^2}$. The error bars are plotted on top of their corresponding magnetization values.

Our results demonstrate that, with a detection distance up to 6.7 mm, we have achieved a spatial resolution of 23 μm. The magnetization, and hence the number of nanoparticles, is accurate within 1.8% for roughly 30 nL of the sample. It indicates a detection limit of about 500 pL of the sample being used here. With micrometer resolution and a subnanoliter detection limit, our technique fills the gap between microscopic magnetic imaging and long-distance magnetic sensing.

It consequently opens new avenues for magnetic imaging applications: magnetic nanoparticles being used in practical applications can now be imaged with high resolution and low detection limit. Of particular interest is the imaging of magnetic markers employed in lab-on-a-chip devices.[13] Our technique should be able to identify the channels that contain magnetic particles and reveal the amount of magnetically labeled biochemical entities therein.

Our magnetometer offers several unique features compared to other related techniques.[14] The operation temperature of the device is 37 °C, which is compatible with biomedical assay analysis and in vivo imaging. Geometrically, the small detector size and overall compact design, which is less than a tenth of the volume of similar instruments, render it more viable for practical conditions. In addition, the stability of the instrument is significantly better than previous related designs, probably because of the use of a stabilized Cs laser: it can function for many hours before the sensitivity needs to be readjusted. Coupled with a fast measurement time of 30 ms and no signal averaging, the path of the magnetic particles can thus be continuously monitored for an extended period, which is valuable for biomedical processes with slow dynamics.

The sensitivity of our magnetometer may be further improved.[15] It is worthwhile to estimate the intrinsic sensitivity of our atomic magnetometer, with a given size of 125 μL and a fixed operating temperature of 37 °C. Based on modeling by Kitching and co-workers,[16] our sensitivity can reach 1 $fT/(Hz)^{1/2}$ when spin-exchange relaxation between atoms is the limiting decoherence factor, and 0.1 $fT/(Hz)^{1/2}$ when the magnetometer is operated in a spin-exchange relaxation-free regime. A 0.1 $fT/(Hz)^{1/2}$ sensitivity will lead to a spatial resolution of 2 μm or a detection limit of a few hundred magnetic nanoparticles, which corresponds to several zeptomoles of magnetically labeled biochemical entities.

For applications in which the sample must be stationary (e.g., when large biomedical systems or geophysical objects are involved), imaging can be achieved by scanning the magnetometer. It is also possible to assemble a two-dimensional array for better signal-to-noise ratio and detection efficiency, especially when multiple samples are being imaged. Three-dimensional magnetic imaging is also possible with a scanning magnetometer array. The sensitive axis can be altered by changing the direction of the bias magnetic field and propagation of the laser beam.

In conclusion, we have descrbed a scanning imaging method using an atomic magnetometer for imaging magnetic nanoparticles. The combination of approximately 20 μm resolution, nearly 1 cm detection distance, and picoliter-range detection limit makes this technique uniquely suited for practical applications of magnetic nanoparticles. Both the resolution and detection limit have much room for improvement, which will be the focus for future research. In addition, the integration of all the optical and mechanical components of the magnetometer is also important for enhanced applicability for routine use in biomedical research.

Experimental Section

The atomic magnetometer was based on the D1 transition of cesium atoms that are contained in a cubic cell with a volume of 125 μL. The incident laser power was 8 μW. A capillary loaded with approximately 30 nL of amine-coated magnetic particles (Sigma–Aldrich I-7643) was placed on a sample holder, which was located several millimeters from the atomic detector. The number of the magnetic particles was estimated to be 7×10^5 based on the concentration of the particles provided by the manufacturer. Prior to the measurements, the magnetic nanoparticles were magnetized by approaching the pole face of a permanent magnet vertically. The motion of the sample was achieved by using an automated linear actuator for *x*-axis scans and a pair of motorized nanopositioning stages for *d*-axis movements. The magnetic field from the sample was measured by monitoring the magneto-optical resonance on the polarization rotation of the laser beam.[14] The sensitivity of the atomic magnetometer is approximately 200 $fT/(Hz)^{1/2}$. The integration time for each data point is 30 ms.

Received: April 20, 2009
Published online: June 27, 2009

Keywords: atomic magnetometry · biological markers · imaging · magnetic properties · nanotechnology

[1] a) J.-M. Nam, C. S. Thaxton, C. A. Mirkin, *Science* **2003**, *301*, 1884 – 1886; b) Y. Suzuki, C. H. Cunningham, K.-I. Noguchi, I. Y. Chen, I. L. Weissman, A. C. Yeung, R. C. Robbins, P. C. Yang, *Magn. Reson. Med.* **2008**, *60*, 1269 – 1275; c) T. Neuberger, B. Schöpf, H. Hofmann, M. Hofmann, B. von Rochenberg, *J. Magn. Magn. Mater.* **2005**, *293*, 483 – 496; d) J. W. M. Bulte, D. L. Kraitchman, *NMR Biomed.* **2004**, *17*, 484 – 499; e) L.-S. Bouchard, M. S. Anwar, G. L. Liu, B. Hann, Z. H. Xie, J. W. Gray, X. Wang, A. Pines, F. F. Chen, *Proc. Natl. Acad. Sci. USA* **2009**, *106*, 4085 – 4089.

[2] X. Lou, J. Qian, Y. Xiao, L. Viel, A. E. Gerdon, E. T. Lagally, P. Atzberger, T. M. Tarasow, A. J. Heeger, H. T. Soh, *Proc. Natl. Acad. Sci. USA* **2009**, *106*, 2989 – 2994.

[3] M. V. Yezhelyev, *Lancet Oncol.* **2006**, *7*, 657 – 667.

[4] a) S. Schreiber, M. Savla, D. V. Pelekhov, D. F. Iscru, C. Selcu, P. C. Hammel, G. Agarwal, *Small* **2008**, *4*, 270 – 278; b) M. Albrecht, V. Janke, S. Sievers, U. Siegner, D. Schüler, U. Heyen, *J. Magn. Magn. Mater.* **2005**, *290–291*, 269 – 271; c) U. Kaiser, A. Schwarz, R. Wiesendanger, *Nature* **2007**, *446*, 522 – 525; d) D. Rugar, R. Budakian, H. J. Mamin, B. W. Chui, *Nature* **2004**, *430*, 329 – 332.

[5] B. Srinivasan, Y. Li, Y. Jing, Y.-H. Xu, X. Yao, C. Xing, J.-P. Wang, *Angew. Chem.* **2009**, *121*, 2802 – 2805; *Angew. Chem. Int. Ed.* **2009**, *48*, 2764 – 2767.

[6] a) B. Gleich, J. Weizenecker, *Nature* **2005**, *435*, 1214 – 1217; b) D. Baumgarten, M. Liehr, F. Wiekhorst, U. Steinhoff, P. Münster, P. Miethe, L. Trahms, J. Haueisen, *Med. Biol. Eng. Comput.* **2008**, *46*, 1177 – 1185.

[7] O. Veiseh, C. Sun, J. Gunn, N. Kohler, P. Gabikian, D. Lee, N. Bhattarai, R. Ellenbogen, R. Sze, A. Hallahan, J. Olson, M. Zhang, *Nano Lett.* **2005**, *5*, 1003 – 1008.

[8] a) R. Kopelman, Y.-E. L. Koo, M. Philbert, B. A. Moffat, G. R. Reddy, P. McConville, D. E. Hall, T. L. Chenevert, M. S. Bhojani, S. A. Buck, A. Rehemtulla, B. D. Ross, *J. Magn. Magn. Mater.* **2005**, *293*, 404 – 410; b) A. Ito, M. Shinkai, H. Honda, T. Kobayashi, *J. Biosci. Bioeng.* **2005**, *100*, 1 – 11.

[9] a) I. K. Kominis, T. W. Kornack, J. C. Allred, M. V. Romalis, *Nature* **2003**, *422*, 596 – 599; b) D. Budker, D. F. Kimball, S. M. Rochester, V. V. Yashchuk, M. Zolotorev, *Phys. Rev. A* **2000**, *62*, 043403; c) D. Budker, M. V. Romalis, *Nat. Phys.* **2007**, *3*, 227 – 234.

[10] a) H. E. Horng, S. Y. Yang, Y. W. Huang, W. Q. Jiang, C.-Y. Hong, H. C. Yang, *IEEE Trans. Appl. Supercond.* **2005**, *15*, 668–671; b) L. E. Fong, J. R. Holzer, K. K. McBride, E. A. Lima, F. Baudenbacher, M. Radparvar, *Rev. Sci. Instrum.* **2005**, *76*, 053703; c) Y. R. Chemla, H. L. Grossman, Y. Poon, R. McDermott, R. Stevens, M. D. Alper, J. Clarke, *Proc. Natl. Acad. Sci. USA* **2000**, *97*, 14268–14272.

[11] M. Pannetier, C. Fermon, G. Le Goff, J. Simola, E. Kerr, *Science* **2004**, *304*, 1648–1650.

[12] S.-J. Xu, M. H. Donaldson, A. Pines, S. M. Rochester, D. Budker, V. V. Yashchuk, *Appl. Phys. Lett.* **2006**, *89*, 224105.

[13] a) N. Pamme, *Lab Chip* **2006**, *6*, 24–38; b) B. Le Drogoff, L. Clime, T. Veres, *Microfluid. Nanofluid.* **2008**, *5*, 373–381.

[14] S.-J. Xu, S. M. Rochester, V. V. Yashchuk, M. H. Donaldson, D. Budker, *Rev. Sci. Instrum.* **2006**, *77*, 083106.

[15] D. Yu, N. Garcia, S.-J. Xu, *Concepts Magn. Reson. Part A* **2008**, *34*, 124–132.

[16] V. Shah, S. Knappe, P. D. D. Schwindt, J. Kitching, *Nat. Photonics* **2007**, *1*, 649–652.

